



HAL
open science

A non-local shell model of hydrodynamic and magnetohydrodynamic turbulence

Franck Plunian, Rodion Stepanov

► **To cite this version:**

Franck Plunian, Rodion Stepanov. A non-local shell model of hydrodynamic and magnetohydrodynamic turbulence. *New Journal of Physics*, 2007, 9 (art. no. 294), pp.NIL_52-NIL_77. 10.1088/1367-2630/9/8/294 . insu-00347599

HAL Id: insu-00347599

<https://insu.hal.science/insu-00347599>

Submitted on 19 Aug 2023

HAL is a multi-disciplinary open access archive for the deposit and dissemination of scientific research documents, whether they are published or not. The documents may come from teaching and research institutions in France or abroad, or from public or private research centers.

L'archive ouverte pluridisciplinaire **HAL**, est destinée au dépôt et à la diffusion de documents scientifiques de niveau recherche, publiés ou non, émanant des établissements d'enseignement et de recherche français ou étrangers, des laboratoires publics ou privés.



Distributed under a Creative Commons Attribution 4.0 International License

OPEN ACCESS

A non-local shell model of hydrodynamic and magnetohydrodynamic turbulence

To cite this article: F Plunian and R Stepanov 2007 *New J. Phys.* **9** 294

View the [article online](#) for updates and enhancements.

You may also like

- [Magnetohydrodynamic Turbulence](#)
Dieter Biskamp
- [Mixing and turbulent mixing in fluids, plasma and materials: summary of works presented at the 3rd International Conference on Turbulent Mixing and Beyond](#)
Serge Gauthier, Christopher J Keane, Joseph J Niemela et al.
- [Plasma and Fluid Turbulence: Theory and Modelling](#)
A Yoshizawa, S I Itoh and K Itoh

A non-local shell model of hydrodynamic and magnetohydrodynamic turbulence

F Plunian^{1,2,4} and R Stepanov³

¹ Laboratoire de Géophysique Interne et Tectonophysique, CNRS, Université Joseph Fourier, Maison des Géosciences, BP 53, 38041 Grenoble Cedex 9, France

² Laboratoire des Écoulements Géophysiques et Industriels, CNRS, Université Joseph Fourier, INPG, BP 53, 38041 Grenoble Cedex 9, France

³ Institute of Continuous Media Mechanics, Korolyov 1, 614013 Perm, Russia

E-mail: Franck.Plunian@ujf-grenoble.fr and rodion@icmm.ru

New Journal of Physics **9** (2007) 294

Received 15 December 2006

Published 31 August 2007

Online at <http://www.njp.org/>

doi:10.1088/1367-2630/9/8/294

Abstract. We derive a new shell model of magnetohydrodynamic (MHD) turbulence in which the energy transfers are not necessarily local. Like the original MHD equations, the model conserves the total energy, magnetic helicity, cross-helicity and volume in phase space (Liouville's theorem) apart from the effects of external forcing, viscous dissipation and magnetic diffusion. The model of hydrodynamic (HD) turbulence is derived from the MHD model setting the magnetic field to zero. In that case the conserved quantities are the kinetic energy and the kinetic helicity. In addition to a statistically stationary state with a Kolmogorov spectrum, the HD model exhibits multiscaling. The anomalous scaling exponents are found to depend on a free parameter α that measures the non-locality degree of the model. In freely decaying turbulence, the infra-red spectrum also depends on α . Comparison with theory suggests using $\alpha = -5/2$. In MHD turbulence, we investigate the fully developed turbulent dynamo for a wide range of magnetic Prandtl numbers in both kinematic and dynamic cases. Both local and non-local energy transfers are clearly identified.

⁴ Author to whom any correspondence should be addressed.

Contents

1. Introduction	2
2. General concept	4
2.1. The model	4
2.2. All possible interactions	5
2.3. Evaluation of α	5
2.4. Energy transfers	6
2.5. Energy fluxes	8
2.6. HD forcing and initial conditions	9
3. Results	10
3.1. HD intermittency	10
3.2. HD and MHD energy spectra	10
3.3. MHD energy fluxes	14
3.4. MHD energy transfers	15
4. Discussion	17
Acknowledgments	18
Appendix A. Possible triads in logarithmic shell models	19
Appendix B. Expressions of the energy transfers	20
Appendix C. Energy transfer results	20
References	24

1. Introduction

Pioneering shell models of hydrodynamic (HD) turbulence were developed in the seventies [1]–[5], aiming at reproducing the main turbulence features with a low order model of equations. Such shell models were also called wave packet representations [6] for the Fourier space is logarithmically divided into shells of logarithmic width λ such that each wave packet (or shell) k_n is defined by $k_0\lambda^{n-1} < k \leq k_0\lambda^n$. These models are local in the sense that each shell interacts with only the first neighbours like the DN model (named after Desnyansky and Novikov [4]), or the first two neighbours like the GOY model (named after Gledzer, Ohkitani and Yamada [3, 7]). The latter has been intensively studied, one of the main issues being that its cascade dynamics are characterized by anomalous scaling exponents as in turbulence intermittency (for a review, see e.g. [8]–[11] and references therein). This model has been subjected to improvements leading to the so-called Sabra model [12]–[14] or extensions using wavelet decomposition [15]. The GOY and subsequently Sabra models have been used in different contexts like convection [16] or rotation [17]. It has been shown [18] that the DN model is a spectral reduction of the GOY model, showing in some sense the consistency of one model against the other.

To our knowledge only one non-local shell model of turbulence has been developed so far, by Zimin and Hussain [19], projecting the Navier–Stokes equations onto a wavelet basis, and reducing the number of variables from statistical assumptions. In such a non-local model each shell may interact with any other shell. Since then, the original model has been improved by Zimin in order to include left- or right-handed polarity of the solenoidal basis functions as in the complex helical wave decomposition, and used by Melander and Fabijonas [20]–[22].

The extension of shell models to magnetohydrodynamic (MHD) turbulence has been done including either first neighbours interactions [23]–[26] or first two neighbours interactions [27]–[31] possibly including Hall effects [32, 33]. However there are a number of situations in MHD turbulence in which assuming the locality of energy transfers may become somewhat spurious even if the turbulence is considered as isotropic [31]. This is true for example when a large scale external magnetic field is imposed leading to Alfvén waves [34]–[36]. This problem has been tackled using a MHD shell model implementing non-local interactions with the externally imposed magnetic field scale [26]. However it has been shown recently using another method [37] that the other non-local interactions are also important and may rule out the predicted Iroshnikov–Kraichnan $k^{-3/2}$ spectrum. Non-local interactions are also at the heart of the dynamo problem i.e. when the magnetic field is produced by the turbulent motion instead of being externally applied. For example at large values of the magnetic Prandtl number, the magnetic spectrum is expected to peak at scales much smaller than the viscous scale [38]–[40] providing direct evidence of the importance of non-local energy transfers. In the presence of helicity, two possible mechanisms may generate a large scale magnetic field as observed in planets and stars: either a local inverse cascade [41] or a non-local direct transfer from small to large scales as predicted by the mean-field theory [42]. Which mechanism prevails is still not clear. Recently, the importance of non-local interactions was shown in both HD [43] and MHD [44, 45] turbulence. For turbulent dynamo action non-local transfers from large scale kinetic energy to small scale magnetic energy were found [46]. For recent reviews on MHD turbulence and the dynamo problem, see also [47, 48].

In the present paper our aim is to introduce a new shell model of turbulence which is non-local and which can be used either in its HD or MHD form. We shall introduce the MHD model only, the HD one being easily deduced from the former, by setting the magnetic field to zero. Our model can be understood as a non-local version of the Sabra model. This involves similar rules for complex conjugations and imposes a value of shell spacing equal to the golden number. Our first attempt to derive a non-local shell model of MHD turbulence was based on the Zimin model [19]. However we realized that this model was unable to describe the non-local interaction between a large scale velocity and two small neighbouring scales of the magnetic field. We believe that the one which is described here is more relevant to actual isotropic MHD turbulence.

Finally let us point out the relevance of deriving one more shell model while computers allow us to carry out simulations of the Navier–Stokes and induction equations. Of course compared to the original equations such an approach suffers from intrinsic weaknesses like the absence of structures and phase coherence effects. However we believe that shell models may help to understand the role of essential ingredients of the original equations like conservation laws, the degree of non-linearity, the role of local/non-local interactions, etc. They also permit investigation of ranges of magnetic Prandtl numbers far from those achieved in today’s direct numerical simulations. In particular, shell models allow us to consider very small values of viscosity and diffusivity in order to have extended inertial ranges. Finally, though more complex than the local GOY or Sabra model, our non-local shell model is still simple to understand and requires a small amount of computing power.

2. General concept

2.1. The model

The model is defined by the following set of equations

$$\dot{U}_n = ik_n [Q_n(U, U, a) + Q_n(B, B, -a)] - \nu k_n^2 U_n + F_n, \quad (1)$$

$$\dot{B}_n = ik_n [Q_n(U, B, b) + Q_n(B, U, -b)] - \eta k_n^2 B_n, \quad (2)$$

where

$$Q_n(X, Y, c) = \sum_{m=1}^N T_m [c_m^1 X_{n+m}^* Y_{n+m+1} + c_m^2 X_{n-m}^* Y_{n+1} + c_m^3 X_{n-m-1} Y_{n-1}] \quad (3)$$

represents the non-linear transfer rates. The parameters ν and η are respectively the kinematic viscosity and the magnetic diffusivity, F_n is the forcing of turbulence, and $k_n = \lambda^n$. Though the choice of the value of λ is rather arbitrary (provided it is larger than unity), we show in section 2.2 that the golden number is the minimum shell spacing for which the number of possible interactions is minimum. Thus in some sense it should lead to the most accurate results. In addition, it has been shown [12, 14] that the conservation of quasimomenta within a triad is satisfied only if the shell spacing is equal to the golden number. Therefore we take $\lambda = (1 + \sqrt{5})/2$ in the rest of the paper.

For $N = 1$ in (3), we recognize the local Sabra model. The additional non-local interactions for $N \geq 2$ correspond to all other possible triad interactions except the ones involving two identical scales. Expressions for the kinetic energy E_U and helicity H_U , magnetic energy E_B and helicity H_B , and cross-helicity H_C are given by

$$E_U = \sum_n E_U(n), \quad E_U(n) = \frac{1}{2} |U_n|^2, \quad H_U = \sum_n H_U(n), \quad H_U(n) = \frac{1}{2} (-1)^n k_n |U_n|^2, \quad (4)$$

$$E_B = \sum_n E_B(n), \quad E_B(n) = \frac{1}{2} |B_n|^2, \quad H_B = \sum_n H_B(n), \quad H_B(n) = \frac{1}{2} (-1)^n k_n^{-1} |B_n|^2, \quad (5)$$

$$H_C = \sum_n H_C(n), \quad H_C(n) = \frac{1}{2} (U_n B_n^* + B_n U_n^*). \quad (6)$$

In the inviscid and non-resistive limit ($\nu = \eta = 0$), the total energy $E = E_U + E_B$, magnetic helicity and cross-helicity must be conserved ($\dot{E} = \dot{H}_B = \dot{H}_C = 0$). This leads to the following expression for the coefficients a_m^i and b_m^i :

$$a_m^1 = k_m + k_{m+1}, \quad a_m^2 = \frac{-k_{m+1} - (-1)^m}{k_m}, \quad a_m^3 = \frac{k_m - (-1)^m}{k_{m+1}}, \quad (7)$$

$$b_m^1 = (-1)^{m+1}, \quad b_m^2 = 1, \quad b_m^3 = -1.$$

In the case of pure HD turbulence (without magnetic field), the coefficients a_m^i are derived from the kinetic energy and helicity conservations ($\dot{E}_U = \dot{H}_U = 0$), leading again to the same expression as (8). The coefficients T_m are free parameters depending on m only, that we choose to be of the form $T_m = k_{m-1}^\alpha / \lambda(\lambda + 1)$. The coefficient $1/\lambda(\lambda + 1)$ is chosen such that the terms for $m = 1$ in Q_n correspond to the local Sabra model. Thus the local Sabra model corresponds to $\alpha = -\infty$.

2.2. All possible interactions

In our shell model we see from (3) that only a discrete number of triads are allowed. For example, Q_n does not contain any term involving interactions between the modes $n + m$ and $n + m + 2$. The reason why there is only a discrete number of allowed triads comes from the fact that the shells are logarithmically spaced and that the geometrical factor λ satisfies

$$\lambda^2 \geq \lambda + 1. \quad (8)$$

To identify all the allowed triads in a shell model, let us consider three vectors $(\mathbf{k}_1, \mathbf{k}_2, \mathbf{k}_3)$ satisfying

$$\mathbf{k}_1 + \mathbf{k}_2 + \mathbf{k}_3 = 0. \quad (9)$$

Assuming that \mathbf{k}_1 and \mathbf{k}_2 belong to shell n and p , we have

$$k_0 \lambda^{n-1} < |\mathbf{k}_1| \leq k_0 \lambda^n, \quad k_0 \lambda^{p-1} < |\mathbf{k}_2| \leq k_0 \lambda^p. \quad (10)$$

From (9), this implies

$$k_0 |\lambda^{n-1} - \lambda^{p-1}| \leq |\mathbf{k}_3| \leq k_0 (\lambda^n + \lambda^p). \quad (11)$$

Now using the inequalities (8) and (11) we can show that \mathbf{k}_3 belongs to shell q which depends on p in the following way:

$$\begin{aligned} p \leq n - 3 &\Rightarrow n - 1 \leq q \leq n + 1, & p = n + 1 &\Rightarrow q \leq n + 2, \\ p = n - 2 &\Rightarrow n - 2 \leq q \leq n + 1, & p = n + 2 &\Rightarrow n \leq q \leq n + 3, \\ p = n - 1 &\Rightarrow q \leq n + 1, & p \geq n + 3 &\Rightarrow p - 1 \leq q \leq p + 1, \\ p = n &\Rightarrow q \leq n + 2. \end{aligned} \quad (12)$$

This is illustrated in figure 1 in the plane (p, q) where the grey (resp. white) squares indicate allowed (resp. not allowed) triads (n, p, q) . The demonstration of (12) is given in appendix A. In figure 1, the terms corresponding to the original Sabra local model are denoted by ‘L’, the additional non-local terms by ‘N’ and the terms of Zimin’s model by ‘Z’. In every case the possible shells (p, q) are symmetric with respect to the diagonal in the (p, q) plane.

2.3. Evaluation of α

There is one free parameter left, α , which corresponds to the non-locality strength. It is not an easy task (if possible at all) to figure out what α should be in the general case. However we tried

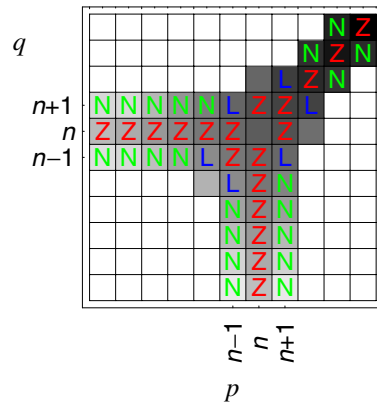


Figure 1. Probability of interactions between three modes belonging to shells n , p and q . The white squares correspond to a null probability.

to estimate it in the case of homogeneous isotropic turbulence (without magnetic field). For that, we took two random vectors \mathbf{k}_1 from shell n , and \mathbf{k}_2 uniformly distributed in whole space, and we calculated the probability that $\mathbf{k}_3 = -(\mathbf{k}_1 + \mathbf{k}_2)$ and \mathbf{k}_2 belong respectively to shells p and q . It is the simplest estimate of the probability that the three modes \mathbf{k}_1 , \mathbf{k}_2 and \mathbf{k}_3 interact together. A high (resp. low) value of this probability is given in figure 1 by the dark (resp. light) colour of the grey squares. In this representation a white square corresponds to a null probability. The probability spectra along the p - and q -directions are found to scale as $k^{-7/2}$ for the ‘L’ and ‘N’ terms and $k^{-5/2}$ for the ‘Z’ terms (which is consistent with the Zimin model [19]). In order to have in (3) terms $T_m c_m^2$ and $T_m c_m^3$ scaling in $k_m^{-7/2}$, we have to take $\alpha = -7/2$. We note that this derivation of α does not prescribe the terms $T_m c_m^1$ (and neither the diagonal terms of figure 1). The latter are determined *a posteriori* from the conservation laws (not included in the probability diagram of figure 1).

On the other hand, in section 3.2.1 we shall find that the value $\alpha = -5/2$ is the most appropriate to describe the spectral exponent of the infra-red kinetic energy spectrum. In the rest of the paper we shall vary the value of α in order to investigate its role in the non-local interactions.

2.4. Energy transfers

To study the non-local interactions, we introduce the transfer rate $\mathcal{T}_{XY}(q, n)$ from X -energy lying in shell q to Y -energy lying in shell n . It can operate only within triads, implying an additional energy Z lying in all other shells p different from q and n . Denoting $T(X_q|Z_p|Y_n)$ the transfer rate from X_q to Y_n and which involves Z_p as a mediator, the transfer rate from X_q to Y_n can then be written as

$$\mathcal{T}_{XY}(q, n) = \sum_{p \neq q, n} T(X_q|Z_p|Y_n). \quad (13)$$

From our model (3) we see that for each couple (X_q, Y_n) , only a discrete number of Z_p can act as mediators. The possible triads are represented schematically in figure 2. Therefore $\mathcal{T}_{XY}(q, n)$

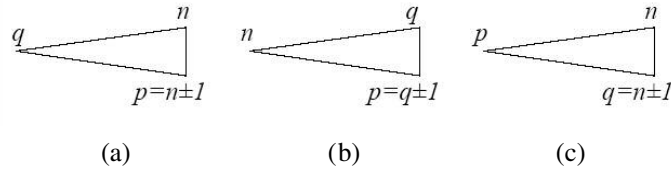


Figure 2. The three types of possible triad (X_q, Z_p, Y_n) : (a) $q \leq n - 1$ and $p = n \pm 1$, (b) $q \geq n + 1$ and $p = q \pm 1$, (c) $q = n \pm 1$ and $p \leq n - 1$. Among these cases those with repeated subscripts ($q = p$, $p = n$ or $q = n$) are forbidden in our model.

takes the following form

$$\mathcal{T}_{XY}(q, n) = \begin{cases} T(X_q|Z_{n+1}|Y_n) + T(X_q|Z_{n-1}|Y_n), & \text{for } q \leq n - 2, \\ T(X_q|Z_{n+1}|Y_n) + \sum_{p \leq n-2} T(X_q|Z_p|Y_n), & \text{for } q = n - 1, \\ T(X_q|Z_{n+2}|Y_n) + \sum_{p \leq n-1} T(X_q|Z_p|Y_n), & \text{for } q = n + 1, \\ T(X_q|Z_{q+1}|Y_n) + T(X_q|Z_{q-1}|Y_n), & \text{for } q \geq n + 2. \end{cases} \quad (14)$$

Now, we have to define $T(X_q|Z_p|Y_n)$ for any X_q, Z_p and Y_n . For that, we can re-write the model (1) and (2) in the following generic form

$$\dot{Y}_n = \sum_{p,q} ik_n M_n(X_q, Z_p) + \dots, \quad (15)$$

where $M_n(X_q, Z_p)$ is a symmetric bilinear form (given in appendix B) representing the quadratic terms. In (15) the dots represent the dissipation and forcing terms appropriate to Y_n .

Now let us denote by $S(X_q, Z_p|Y_n)$ the rate of energy within the triads (X_q, Z_p, Y_n) which is transferred from the couple (X_q, Z_p) to Y_n . It is naturally defined by

$$S(X_q, Z_p|Y_n) = \text{Re} \{ ik_n Y_n^* M_n(X_q, Z_p) \}. \quad (16)$$

As M_n is symmetric, we have

$$S(X_q, Z_p|Y_n) = S(Z_p, X_q|Y_n). \quad (17)$$

In addition, and with the help of (8), we can show that for any triad (X_q, Z_p, Y_n) the following relation is satisfied

$$S(X_q, Z_p|Y_n) + S(Z_p, Y_n|X_q) + S(Y_n, X_q|Z_p) = 0, \quad (18)$$

meaning that the energy is conserved within each triad.

Then we look for $T(X_q|Z_p|Y_n)$ as a linear combination of $S(X_q, Z_p|Y_n)$, $S(Y_n, X_q|Z_p)$ and $S(Z_p, Y_n|X_q)$. As in real MHD turbulence, $T(X_q|Z_p|Y_n)$ must satisfy the following conditions

$$T(X_q|Z_p|Y_n) = -T(Y_n|Z_p|X_q), \quad (19)$$

$$S(X_q, Z_p|Y_n) = T(X_q|Z_p|Y_n) + T(Z_p|X_q|Y_n). \quad (20)$$

The first condition (19) means that the transfer rate from X_q to Y_n and from Y_n to X_q with the same mediator Z_p are of equal intensity but opposite signs. We note that this implies

$$\mathcal{T}_{XY}(q, n) = -\mathcal{T}_{YX}(n, q). \quad (21)$$

The second condition (20) means that in any triad (X_q, Z_p, Y_n) the transfer rate from (X_q, Z_p) to Y_n is equal to the sum of the transfer rates from X_q to Y_n via Z_p and from Z_p to Y_n via X_q . Then combining (17), (18), (19) and (20) we end up with the following expression for T

$$T(X_q|Z_p|Y_n) = \frac{1}{3}[S(X_q, Z_p|Y_n) - S(Y_n, Z_p|X_q)]. \quad (22)$$

Furthermore we can show that the following energy balances at scale n are satisfied

$$\dot{E}_U(n) + \mathcal{D}_U(n) - \mathcal{F}(n) = \sum_q [\mathcal{T}_{UU}(q, n) + \mathcal{T}_{BU}(q, n)], \quad (23)$$

$$\dot{E}_B(n) + \mathcal{D}_B(n) = \sum_q [\mathcal{T}_{UB}(q, n) + \mathcal{T}_{BB}(q, n)], \quad (24)$$

with the kinetic and magnetic dissipation rates in shell n defined by

$$\mathcal{D}_U(n) = \nu k_n^2 |U_n|^2, \quad \mathcal{D}_B(n) = \eta k_n^2 |B_n|^2 \quad (25)$$

and

$$\mathcal{F}(n) = \frac{1}{2}(F_n U_n^* + F_n^* U_n). \quad (26)$$

2.5. Energy fluxes

We define the energy flux $\Pi_{XY}(n)$ as the rate of loss of X -energy lying in the shells $j < n$ to the Y -energy lying in the shell $j \geq n$. Therefore, we have

$$\Pi_{XY}(n) = - \sum_{j=0}^{n-1} \sum_q \sum_p \mathcal{T}_{XY}(q|p|j) \quad (27)$$

$$= - \sum_{j=0}^{n-1} \sum_q \mathcal{T}_{XY}(q, j). \quad (28)$$

The fluxes $\Pi_{UU}(n)$ and $\Pi_{BU}(n)$ coincide respectively with $\sum_{j=0}^{n-1} \text{Im}\{k_j U_j^* Q_j(U, U, a)\}$ and $\sum_{j=0}^{n-1} \text{Im}\{-k_j U_j^* Q_j(B, B, a)\}$. There is no such coincidence for $\Pi_{UB}(n)$ and $\Pi_{BB}(n)$.

The following flux balances are satisfied

$$\sum_{j=0}^{n-1} (\dot{E}_U(j) + \mathcal{D}_U(j) - \mathcal{F}(j)) + \Pi_{UU}(n) + \Pi_{BU}(n) = 0, \quad (29)$$

$$\sum_{j=0}^{n-1} (\dot{E}_B(j) + \mathcal{D}_B(j)) + \Pi_{UB}(n) + \Pi_{BB}(n) = 0. \quad (30)$$

In a statistically stationary case they imply that

$$\Pi_{UU}(n) + \Pi_{BU}(n) + \Pi_{UB}(n) + \Pi_{BB}(n) = - \sum_{j=0}^{n-1} (\mathcal{D}_U(j) + \mathcal{D}_B(j) + \mathcal{F}(j)). \quad (31)$$

In order to investigate the importance of non-local versus local interactions, we define the local part of the fluxes given by (27) in which only the local energy transfer rates $T_{XY}(n \pm 2|n \pm 1|n)$, $T_{XY}(n \pm 1|n \mp 1|n)$ and $T_{XY}(n \pm 1|n \pm 2|n)$ are involved. These fluxes correspond to those of the MHD version of the original (local) Sabra model, taking $N = 1$ in (3). The non-local parts of the fluxes are defined as the total fluxes minus their local parts.

2.6. HD forcing and initial conditions

2.6.1. Forced turbulence. For both HD and MHD cases a HD forcing is applied at scale n_f and n_{f+1} with $n_f = 0$. It is of the form $F_n = A_n e^{i\phi_n(t)}$ where $\phi_n(t) \in [0, 2\pi]$ is constant during time intervals t_c , the constant value changing randomly from one time interval to the next. In this way we obtain a statistically constant injection rate equal to $\epsilon = A_n^2 t_c$. We chose $t_c = 10^{-2}$ for it is smaller than the turn-over time at the injection scale and larger than the viscous characteristic time.

For some arbitrary initial conditions on U_n of small intensity we let the HD evolve until it reaches some statistically stationary state. For the MHD case, some small intensity of B_n is subsequently introduced on a few modes k_n . Then we solve the full problem until a statistically stationary MHD state is reached. We stress that we never apply any magnetic forcing. In all the cases that we considered in the present paper the magnetic field is generated spontaneously from the interactions with the flow, by the so-called dynamo action. This requires a sufficiently intense flow, otherwise the magnetic field just decays. In other words we consider here flows which are much above the dynamo instability threshold. The time of integration needed to obtain good statistics depends on ν and η but is typically several hundreds of the turn-over time at the forcing scale. We define the magnetic Prandtl number as the ratio $P_m = \nu/\eta$.

2.6.2. Freely decaying turbulence. To study the HD freely decaying turbulence (without forcing), we tried different initial conditions. Either we just took some initial condition on two shells ($n = 0$ and $n = 1$) and let the system evolve dynamically; or we started from an initial state derived from a statistically stationary solution of the forced problem. Both initial conditions give the same qualitative results. We also studied the freely decaying MHD turbulence. In that case the initial condition for the magnetic field is taken on two shells only. Though the flow is freely decaying, it is sufficiently intense (at least for some time) to generate a magnetic field by dynamo action.

3. Results

3.1. HD intermittency

Here we consider the case of forced turbulence without magnetic field. The spectra are represented in figure 5 for different values of α (black curves, kinematic case). With slopes in $k_n^{-2/3}$ ($k^{-5/3}$ in three-dimensional (3D) spectral space), they are Kolmogorov-like. In addition, we know that anomalous scaling exponents have been found in both local GOY and Sabra models [12]–[14], [49]–[54]. It is therefore of interest to investigate how the additional non-local interactions may change these anomalous exponents. In the inertial range the scaling exponents ζ_p characterize the statistical moments $\langle |u_n|^p \rangle$ dependence on the wavenumber k_n :

$$\langle |u_n|^p \rangle \propto k_n^{-\zeta_p}. \quad (32)$$

It has been shown that they deviate from the Kolmogorov's mean field theory $\zeta_p = p/3$ as p increases which is interpreted as evidence of intermittency. The determination of the scaling exponents is a delicate matter as its accuracy depends on the inertial range extent (i.e. on ν), on the number of shells N and on the number of samples used for the statistics. Here we take $\nu = 10^{-8}$, $N = 50$ and 10^8 time steps. In addition, different methods have been derived to reach accurate estimates. Here we follow the method proposed by Leveque and She [54]. Due to oscillations peculiar to shell models they suggest considering the quantity

$$\Pi_n = (u_{n-1}u_nu_{n+1})^{1/3} \quad (33)$$

instead of u_n . Then they define the relative scaling exponents as

$$\langle |\Pi_n|^p \rangle \propto \langle |\Pi_n|^3 \rangle^{\zeta_p/\zeta_3}. \quad (34)$$

The corresponding scaling exponents calculated from our model are plotted in figure 3. For $\alpha = -\infty$ our model is equivalent to the Sabra local model and we find that the anomalous scaling exponents differ by less than 3% from the values calculated by L'vov *et al* [12]. For the other values of α , we observe that increasing the non-locality leads to scaling exponents closer to $p/3$.

3.2. HD and MHD energy spectra

3.2.1. Freely decaying turbulence. In this section we study the freely decaying turbulence (no forcing) without (HD) and with (MHD) magnetic field. The results are presented in figure 4 for $\nu = 10^{-6}$ and different values of α and P_m . The top row corresponds to HD turbulence and the three rows below to MHD turbulence. The kinetic (magnetic) spectra are plotted with grey (red) dots at different times. The time sample at which the spectra are plotted is $t = 1, 2, 10, 100, 200$. The dots corresponding to $t = 200$ are the darkest and smallest. Finally we paid attention to take a sufficient number of shells in such a way that the infra-red cut-off corresponds to energies smaller than 10^{-10} . This is true for all the plots of figure 4, even if the largest scales are not necessarily represented. As mentioned in section 2.6 we considered different initial conditions for the flow without finding qualitative differences. Let us then consider the initial conditions applied to two neighbour large scale shells (here $n = 0$ and $n = 1$).

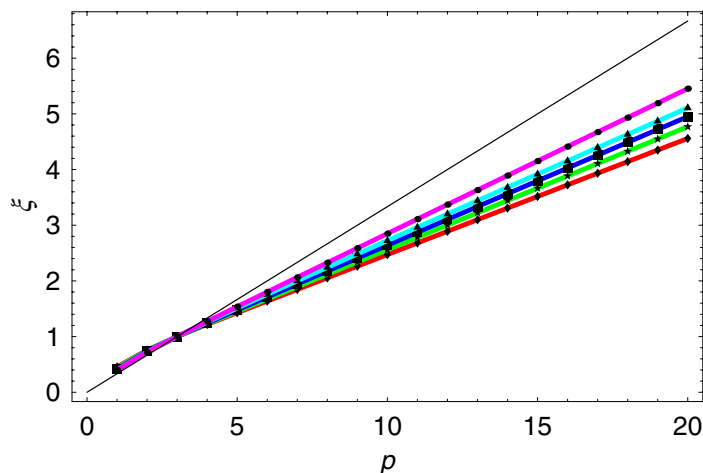


Figure 3. Estimate of the scaling exponents for several values of α . From bottom to top, $\alpha = -\infty, -5/2, -3/2, -1, -1/2$.

In the MHD case, the initial conditions for the field are chosen at the same two scales as the flow ($n = 0$ and $n = 1$) and such that the initial cross-helicity is zero (indeed we found that an initial cross-helicity different from zero would lead to poorly defined inertial ranges of U_n and B_n). Though the turbulent flow is freely decaying, it is sufficiently intense to amplify the magnetic field by dynamo action. For some transient time the magnetic energy grows during the so-called kinematic regime while the magnetic spectrum extends to all scales. After this kinematic regime the magnetic energy saturates and a dynamical balance between the flow and the magnetic field occurs, both being freely decaying. The MHD plots of figure 4 correspond to this saturation regime.

We observe that changing α does not change the spectral exponent of the inertial range for both kinetic and magnetic spectra. It compares well with the Kolmogorov scaling $k_n^{-2/3}$ ($k^{-5/3}$ in spectral space) which is represented by the straight line with negative slope in each plot. On the other hand, changing α drastically changes the infra-red spectral exponents (at large scale). The kinetic and magnetic infra-red spectral exponents are indicated by the two straight lines with positive slopes in each plot. In table 1 they are indicated for both quantities and for the different values of α that are considered. We note that we always find a difference of 2 units between the magnetic and kinetic spectral exponents.

We understand these infra-red spectral exponents as the result of non-local energy transfer in low wavenumbers k_n (with $n \ll 0$) through some interaction between the two initial condition modes k_0 and k_1 .

From the nonlinear transfer rates (3) we find that the time derivative of the infra-red kinetic energy is dominated by the term $T_{-n} a_{-n}^1 U_0^* U_1 U_n^*$. This implies that the kinetic infra-red spectrum scales like $k_n^{-2\alpha}$ in agreement with the values given in table 1. In real 3D freely decaying HD turbulence, the infra-red spectrum results from two leading effects, one corresponding to spectral backscatter (or non-local eddy noise) and the other to eddy viscosity [55]. For a sharply peaked initial energy spectrum the backscatter dominates leading to a k^4 infra-red spectrum [56]. In our model this corresponds to having a k_n^5 kinetic infra-red spectrum which is obtained for $\alpha = -5/2$. Besides, this is in agreement with the infra-red spectrum obtained with Zimin's model [22].

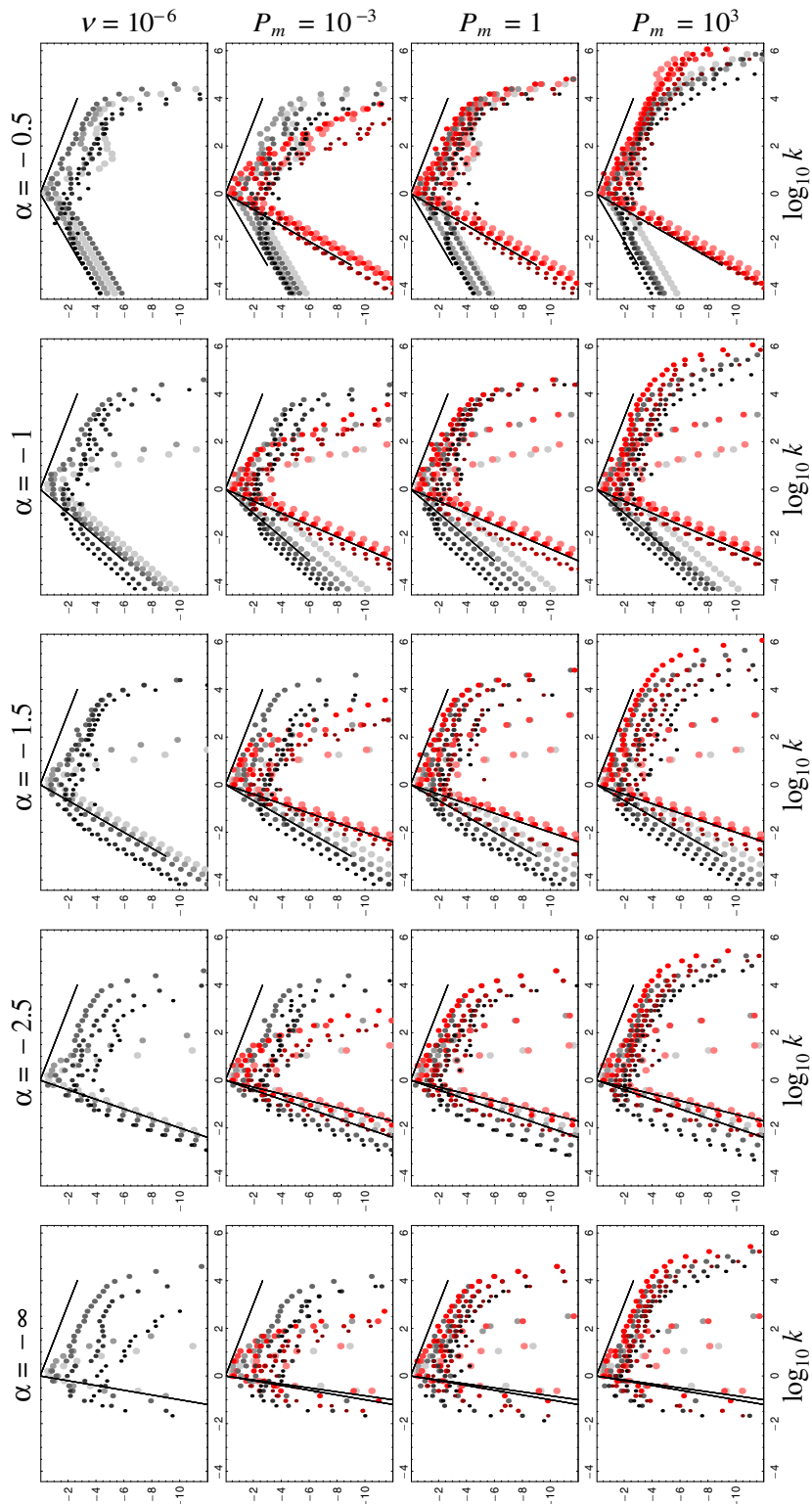


Figure 4. On top: freely decaying turbulence for $\nu = 10^{-6}$. From second to fourth row: freely decaying MHD turbulence for three values of P_m ($\nu = 10^{-6}$). Each column corresponds to a given value of α .

Table 1. Kinetic and magnetic infra-red spectral exponents for several values of α .

$\alpha =$	$-\infty$	-2.5	-1.5	-1	-0.5
Kinetic	10	5	3	2	1
Magnetic	12	7	5	4	3

With the same argument as above we find that the time derivative of the infra-red magnetic energy is dominated by the term $T_{-n} b_{-n}^1 X_0^* Y_1 B_n^*$ implying that $B_n^2 \propto k_n^{-2\alpha+2}$ which again is in agreement with the values given in table 1. The difference of 2 units in the magnetic and kinetic spectral exponents comes from the ratio $|a_n^1/b_n^1| \propto k_n$. Infra-red properties of MHD turbulence have been studied in the case of applied random forces and currents [57] and therefore are not directly applicable to our problem here (no forcing). Finally we know from [41] that injection of magnetic helicity also leads to infra-red magnetic spectra in k^6 . This would correspond to again taking $\alpha = -5/2$ in our model.

The Sabra model, corresponding here to $\alpha = -\infty$ and no magnetic field, leads to a spectral exponent in k_n^{10} (k^9 in 3D spectral space) which is inconsistent with the theoretical predictions [55]. This drastic difference between the local and non-local models emphasizes the importance of including the non-local interactions.

3.2.2. Forced turbulence. With a HD forcing at some given scales (here k_0 and k_1), if there is no cut-off scale above which the system is not solved, a statistically stationary state is never achieved. The kinetic spectrum is then made up of four ranges. From large to small scales, they are: (i) the infra-red range with the same spectral exponent as in freely decaying turbulence, (ii) a range between the infra-red and the forcing scale in which the spectrum is flat (k^{-1} in 3D spectral space), (iii) the inertial range with a Kolmogorov spectrum and (iv) the viscous range in which the energy is dissipated. Contrary to the ranges (iii) and (iv) which are statistically stationary, the range (ii) extends to larger scales versus time and with a time scale which depends on α . As we are interested in statistically stationary states in the rest of the paper, we impose a cut-off at k_0 without calculating the larger scales. We end up with the ranges (iii) and (iv) only.

In figure 5 both kinetic and magnetic energy spectra are plotted for three values of P_m and both kinematic and saturated dynamo regimes. In each plot, the curves correspond to different values of α . In the kinematic regime (top plots) the Lorentz forces corresponding to the term $Q_n(B, B, -a)$ are small and can be neglected in the energy balance. Then the magnetic energy grows exponentially at any scale. The magnetic spectra are thus normalized by the maximum value of $E_B(n)$. In the saturated regime (bottom plots), the Lorentz forces act back onto the flow, leading to statistically stationary kinetic and magnetic energies.

In both kinematic and dynamic regimes and for $P_m \leq 1$ (left and middle plots of figure 5), the effect of α is not really significant. The kinetic spectra (black curves) are almost not sensitive to non-local interactions showing that HD interactions are mostly local as predicted by the Kolmogorov cascade. Besides the kinetic spectra always scale as $k_n^{-2/3}$ ($k^{-5/3}$ in the spectral space) in the inertial range. We see some non-local effects on the magnetic spectra (colour curves) which spread towards large scales or even small scales for $P_m = 10^{-3}$. However, the scale for which the magnetic spectrum is at maximum does not change and is roughly equal to $k_\eta \approx k_\nu P_m^{3/4}$ as again predicted by Kolmogorov arguments (see e.g. [31]).

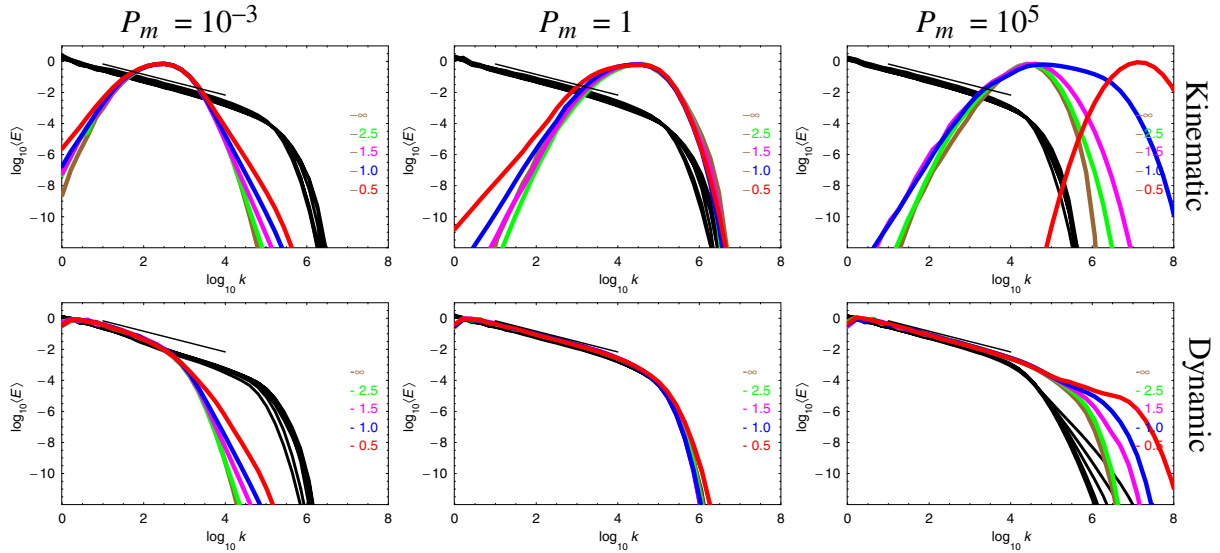


Figure 5. Spectra of kinetic (black curves) and magnetic (colour curves) energy for three values of P_m (from left to right $P_m = 10^{-3}$, 1 and 10^5) and several values of α (indicated by the labels). The spectra on top (resp. bottom) correspond to the kinematic (resp. dynamic) regime.

On the other hand, the non-local effects are much more significant for $P_m > 1$ (plots on the right), mainly for the magnetic spectra at scales smaller than the viscous scales ($k_n \geq k_\nu$) and for $\alpha > -1$. In the kinematic regime the maximum of the magnetic energy spectrum occurs at scales smaller than $k_\nu P_m^{3/4}$ when $\alpha > -1$. In the dynamic regime some magnetic bottleneck appears. To understand why this is so, let us first recall that the flow scale which produces magnetic field in the most efficient way is the one for which the shear is the largest [31]. In the inertial range the flow shear scales as $k_n u_n \propto k_n^{2/3}$, and it is then maximum for $k_n \approx k_\nu$. Therefore the non-local interactions relevant for the magnetic spectrum extension towards smaller scales are mostly those involving U_ν . The non-local terms involving U_ν and generating magnetic energy $E_B(n)$ with $n \gg \nu$ also involve $B_{n\pm 1}$. The corresponding non-local terms in (2) are of the form $k_n(T_{n-\nu} b_{n-\nu}^2 U_\nu^* B_{n+1} + T_{n-\nu-1} b_{n-\nu-1}^3 U_\nu^* B_{n-1})$ which scale as $k_n^{1+\alpha}$. Therefore we understand that for $\alpha + 1 > 0$ the non-local effect may be strong at small scales.

In the kinematic regime, the fact that the magnetic energy spectrum does not peak at scales smaller than k_ν^{-1} for $\alpha < -1$ is in contradiction with previous results [38]–[40]. We attribute this discrepancy to the fact that in our model isotropy is assumed at any scale whereas the scenario described in [39, 40] relies on strong anisotropy at small scales.

3.3. MHD energy fluxes

In this section we set $\alpha = -5/2$ and $\nu = 10^{-8}$ and consider the dynamo saturated regime for three values of $P_m = 10^{-3}$, 1 and 10^4 . The kinetic and magnetic spectra are plotted in the top row of figure 6. Both spectra have inertial ranges of Kolmogorov type, scaling in $k_n^{-2/3}$ (scaling in $k^{-5/3}$ in the spectral space). For $P_m = 10^{-3}$ we identify clearly that the magnetic dissipation scale is much smaller than the viscous dissipation scale. However the distinction between them is not so clear for $P_m = 10^4$.

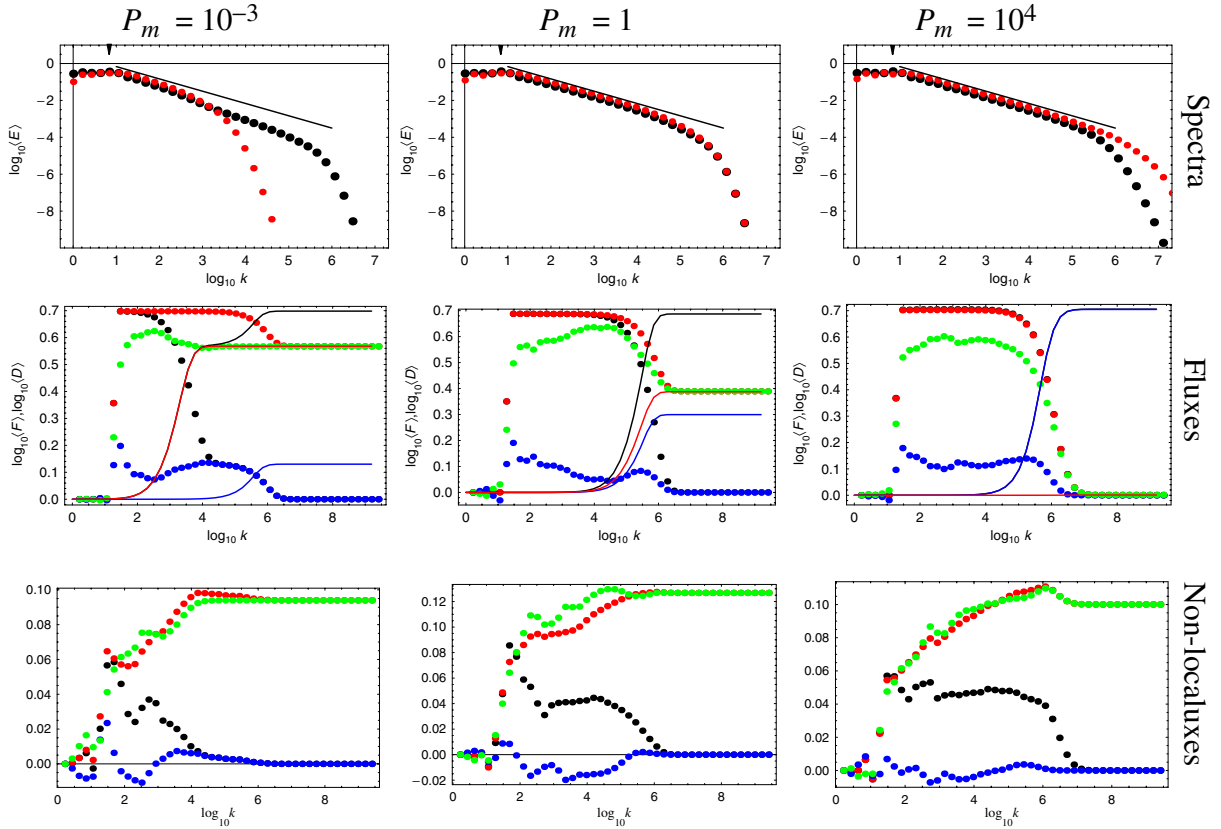


Figure 6. Spectra, total and non-local fluxes for three values of P_m and $\alpha = -5/2$. The kinetic (magnetic) spectra correspond to black (red) dots. The fluxes $\Pi_{UU}(n)$ and $\Pi_{BU}(n)$ are represented by blue and green dots. The red dots correspond to $\Pi_{UU}(n) + \Pi_{BU}(n)$, the black dots to $\Pi_{UU}(n) + \Pi_{BU}(n) + \Pi_{UB}(n) + \Pi_{BB}(n)$. The blue, red and black full lines correspond respectively to $\sum_{j=0}^n \mathcal{D}_U(j)$, $\sum_{j=0}^n \mathcal{D}_B(j)$ and $\sum_{j=0}^n (\mathcal{D}_U(j) + \mathcal{D}_B(j))$.

The total and non-local part of the fluxes are plotted in middle and bottom rows of figure 6. The non-local part of $\Pi_{UU}(n)$ is found to be always much smaller than $\Pi_{UU}(n)$, implying that the energy transfers are mainly local. On the other hand, the importance of the non-local part of $\Pi_{BU}(n)$ versus the local one depends on P_m .

In figure 7 the ratio $\Pi_{BU}^{\text{Non-local}}(n)/\Pi_{BU}^{\text{local}}(n)$ is plotted for the three values of P_m . For $P_m = 10^{-3}$ this ratio is about 20%. For $P_m = 1$ and for scales smaller than the viscous scale $k_\nu \approx 10^6$, this ratio increases up to 50%. Finally, for $P_m = 10^4$ there is a discontinuity at k_ν , the ratio being then equal to -100% at smaller scales.

3.4. MHD energy transfers

The energy transfers $\mathcal{T}_{XY}(q, n)$ have been calculated for several values of P_m , α and shells n for the dynamo saturated regime. The curves are plotted in appendix C. A digest of these curves is plotted in figure 8 in order to discuss some typical results of these energy transfers. The columns from left to right correspond to $P_m = 10^{-3}$, 1 and 10^5 . Each row from top to bottom corresponds

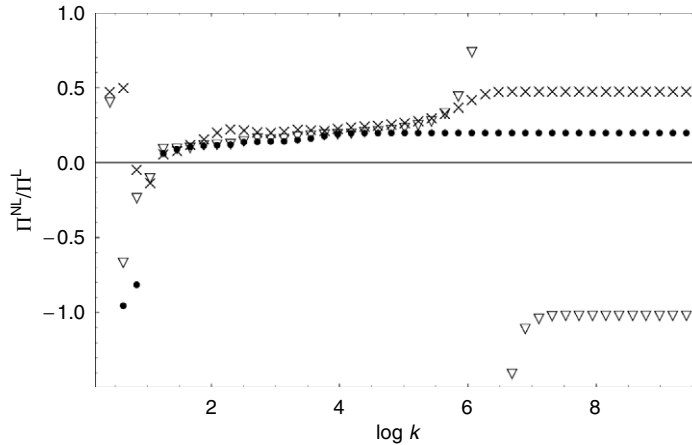


Figure 7. Ratio $\Pi_{BU}^{\text{Non-local}}(n)/\Pi_{BU}^{\text{Local}}(n)$ for $P_m = 10^{-3}$ (dots), 1 (crosses) and 10^4 (triangles).

to $\mathcal{T}_{UU}(q, n)$, $\mathcal{T}_{BU}(q, n)$, $\mathcal{T}_{UB}(q, n)$ and $\mathcal{T}_{BB}(q, n)$ for one given value of n denoted by the black dot. The curves correspond to $\alpha = -\infty$ (green), $-5/2$ (magenta), $-3/2$ (blue) and -1 (red).

For $P_m = 10^{-3}$, the shell n (black dot) belongs to the kinetic inertial range and the magnetic dissipation range. We find that $|\mathcal{T}_{UU}| \gg |\mathcal{T}_{BU}|$, implying that the dominant energy transfer feeding the kinetic energy is a local direct cascade of kinetic energy. In addition we find that \mathcal{T}_{BU} is mainly local and always negative. This means that energy is transferred locally from U_n to B_n (which is consistent with the curve \mathcal{T}_{UB} just below). In addition, we see that the curve of \mathcal{T}_{BU} extends towards larger and larger scales when α goes to zero. Though it is small (up to 20%), its extent over three decades is a clear evidence of non-local transfer from small scale kinetic to large scale magnetic energy. We interpret this as an α -effect in the sense of mean field theory. Finally, though much smaller than \mathcal{T}_{UB} , there is clear evidence of non-local direct cascade of magnetic energy as shown by \mathcal{T}_{BB} .

For $P_m = 1$, the shell n (black dot) belongs to both kinetic and magnetic inertial ranges. We find that $|\mathcal{T}_{BU}|$ and $|\mathcal{T}_{UB}|$ are the main energy transfers and that they are mainly local. In addition, a closer look at \mathcal{T}_{UB} reveals additional transfer from U_q to B_n with $q < n$ extending over one decade, which is consistent with results obtained from 3D direct numerical simulation [46].

For $P_m = 10^5$, the shell n (black dot) is smaller than the kinetic viscous scale and belongs to the magnetic inertial range. We find that $|\mathcal{T}_{UU}| \ll |\mathcal{T}_{BU}|$ implying that the kinetic energy is mainly transferred from magnetic energy. This transfer \mathcal{T}_{BU} is found to be mainly local. The curves of \mathcal{T}_{UB} show clear evidence of non-local transfers. This suggests that the kinetic scales with the largest shear are transferring energy to smaller magnetic scales. However instead of being stocked there, this energy (or at least some part of it) is transferred back locally to kinetic scales belonging to the kinetic viscous range as shown by the curves of \mathcal{T}_{BU} . This energy is then lost by viscous dissipation. This explains why the magnetic energy does not peak at small scales as shown in figure 5 for the dynamic regime. Finally, for $P_m = 1$ and $P_m = 10^5$, \mathcal{T}_{BB} shows evidence of some kind of non-local inverse cascade though much smaller than \mathcal{T}_{UB} .

In figures 9–11 we give some qualitative illustration of the previous interpretation of the results.

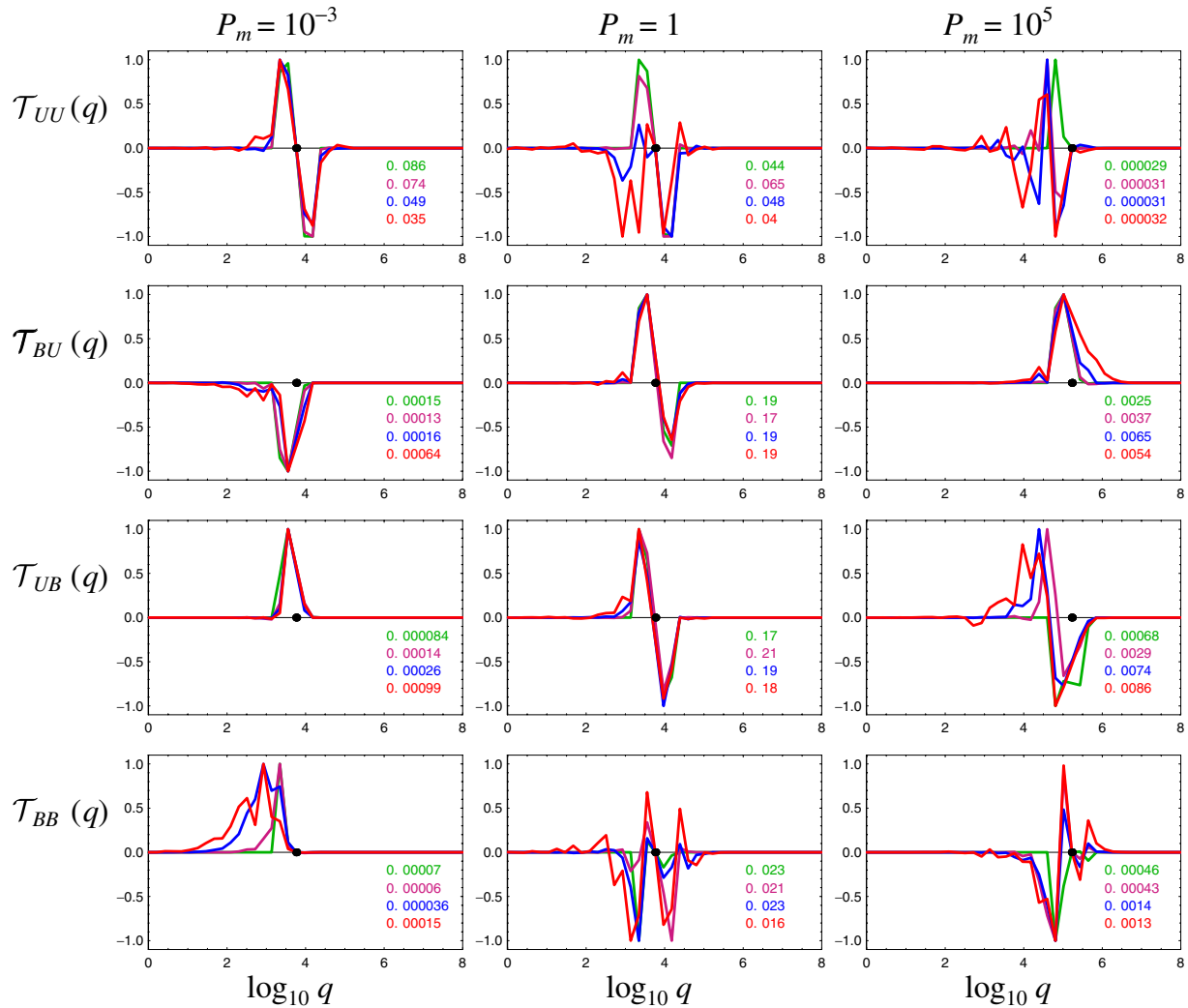


Figure 8. From left to right column, $P_m = 10^{-3}$, 1 , 10^5 . From top to bottom, the plots correspond to $\mathcal{T}_{UU}(q, n)$; $\mathcal{T}_{BU}(q, n)$; $\mathcal{T}_{UB}(q, n)$; $\mathcal{T}_{BB}(q, n)$ for n indicated by the black dot. Each curve corresponds to $\alpha = -\infty$ (green), $-5/2$ (magenta), $-3/2$ (blue) and -1 (red).

4. Discussion

The main originality of the shell model presented in (2) and (3) is that it takes into account all possible non-local interactions between different shells. In essence it is a non-local MHD version of the Sabra model. There is one free parameter left that we call α (which is different from the α -effect of the mean-field dynamo theory) which controls the strength of non-locality of the model.

An estimation of α has been done on the basis of simple probabilistic arguments of possible triad interactions, leading to $\alpha = -7/2$. However, comparing the infra-red kinetic spectrum obtained in freely decaying HD turbulence with theory suggests using $\alpha = -5/2$. In comparison we note that the Sabra model (corresponding here to $\alpha = -\infty$) leads to a much larger infra-red

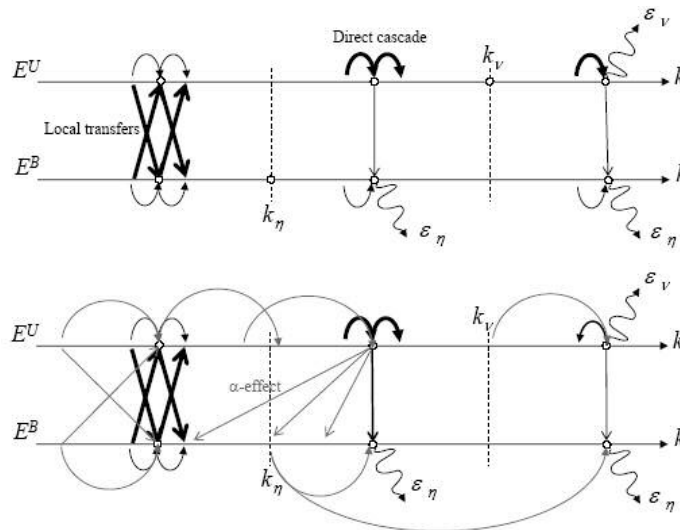


Figure 9. Illustration of the energy transfers for $P_m \ll 1$ for local (top) and non-local (bottom) models. The thickness of the arrow gives some qualitative estimate of the strength of the transfer.

spectral exponent (k^9) than theoretical predictions. In forced HD turbulence, anomalous scaling exponents have been calculated. They are found to depend on α and then on the strength of the non-local interactions.

In a MHD turbulent dynamo we investigated several values of α ranging from $-\infty$ to -0.5 . Several values of P_m have been investigated depending on whether it is lower than, equal to or larger than 1. In order to characterize the energy transfers within any possible triad, the quantities $\mathcal{T}_{XY}(q, n)$ (transfer rate from X -energy lying in shell q to Y -energy lying in shell n) have been derived and plotted versus q for a few values of n . Though most of them are local, several energy transfers have been found to be partially non-local, depending on P_m .

At small P_m we find large scale magnetic energy obtained from smaller scale kinetic energy. We understand such a non-local energy transfer as a mean-field dynamo α -effect. At large P_m we find strong energy transfer from kinetic scales belonging to the inertial range and close to the viscous scale towards smaller magnetic scales. This non-local transfer corresponds to the usual kinematic picture in which the vortices of maximum shear (close to the viscous scale) generate magnetic field of much smaller scales. In addition we find that this magnetic energy is then transferred back locally to kinetic scales in the viscous range where it is lost by viscous dissipation.

Acknowledgments

This work was supported by the Econet Program 10257QL. Multiprocessor computational resources were supported by a special programme of the Russian Academy of Science. RS thanks Basic Research Higher Education (BRHE) post-doctoral fellowship programme (Civilian Research and Development Foundation (CRDF) grant Y2-MP-09-02) for financial support. We thank A Alexakis, P Frick, H Politano and A Schekochihin for fruitful discussions.

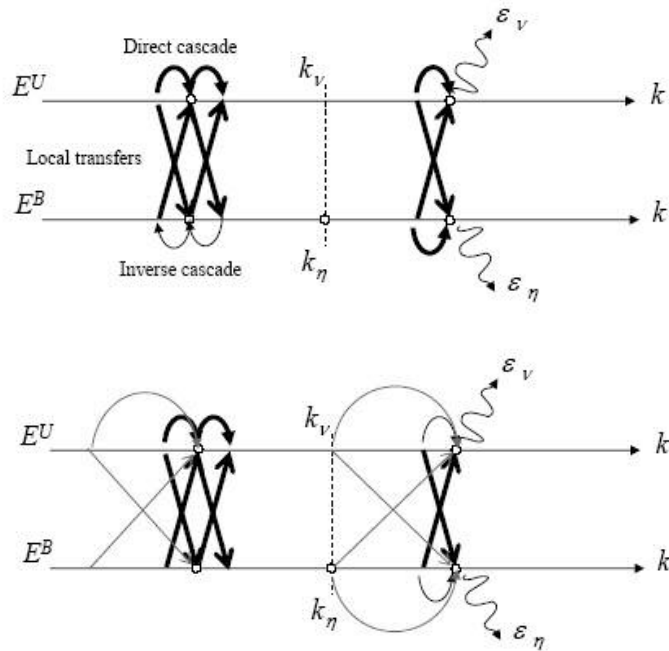


Figure 10. Same as figure 9 but for $P_m = 1$.

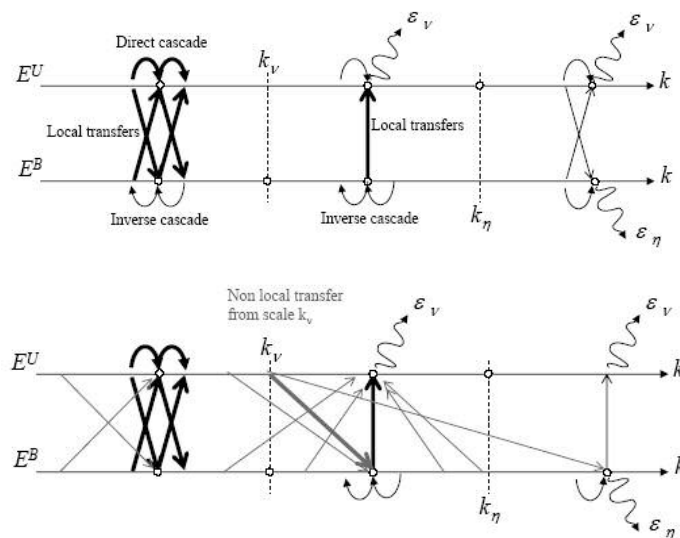


Figure 11. Same as figure 9 but for $P_m \gg 1$.

Appendix A. Possible triads in logarithmic shell models

For a given shell n , we first take benefit from the fact that the triads (n, p, q) and (n, q, p) are identical and then the representation in the plane (p, q) is symmetric with respect to the diagonal. We then limit our demonstration to half of (12).

1. Assuming $p \leq n - 1$, we have $\lambda^n + \lambda^p \leq \lambda^n + \lambda^{n-1}$. Then from (8) and (11) we have $|\mathbf{k}_3| \leq k_0 \lambda^{n+1}$, implying $q \leq n + 1$.
2. For $p = n$, we have $\lambda^n + \lambda^p = 2\lambda^n$. From (8) we have $2 \leq \lambda^2$. Therefore from (11) we have $|\mathbf{k}_3| \leq k_0 \lambda^{n+2}$ and then $q \leq n + 2$.
3. From (8) we have $\lambda^{p+1} - \lambda^p \geq \lambda^{p-1}$. For $p \geq n + 1$ we then have $\lambda^{p+1} - \lambda^p \geq \lambda^n$, implying from (11) that $|\mathbf{k}_3| \leq k_0 \lambda^{p+1}$ and then $q \leq p + 1$.
4. Assuming that $p \leq n - 3$, from (11) we have $|\mathbf{k}_3| \geq k_0 |\lambda^{n-1} - \lambda^{n-4}|$. Then (8) implies $\lambda^{n-1} \geq \lambda^{n-2} + \lambda^{n-3} > \lambda^{n-2} + \lambda^{n-4}$. Then we have $|\mathbf{k}_3| > k_0 \lambda^{n-2} \geq \lambda^{n-1}$ and then $q \geq n - 1$.
5. For $p = n - 2$, from (11) we have $|\mathbf{k}_3| \geq k_0 |\lambda^{n-1} - \lambda^{n-3}|$. From (8) we have $\lambda^{n-1} - \lambda^{n-3} \geq \lambda^{n-2}$, implying $|\mathbf{k}_3| \geq \lambda^{n-2}$ and then $q \geq n - 2$.

Appendix B. Expressions of the energy transfers

The energy transfer (22) can be written with the help of (16) in the form

$$T(X_q|Z_p|Y_n) = \frac{1}{3} \text{Re} \left\{ ik_n Y_n^* M_n(X_q, Z_p) - ik_q X_q^* M_q(Y_n, Z_p) \right\}. \quad (\text{B.1})$$

The symmetric bilinear form $M_n(X_q, Z_p)$ is defined as follows

$$M_n(U_q, U_p) = L_n(U_q, U_p, +a) + L_n(U_p, U_q, +a), \quad (\text{B.2})$$

$$M_n(B_q, B_p) = L_n(B_q, B_p, -a) + L_n(B_p, B_q, -a), \quad (\text{B.3})$$

$$M_n(U_q, B_p) = L_n(U_q, B_p, +b) + L_n(B_p, U_q, -b), \quad (\text{B.4})$$

$$M_n(B_q, U_p) = L_n(B_q, U_p, -b) + L_n(U_p, B_q, +b), \quad (\text{B.5})$$

with $L_n(X_p, Y_q, c)$ given by

$$L_n(X_q, Z_p, c) = \begin{cases} T_{p-q} c_{p-q}^3 X_q Z_p & \text{for } q \leq n - 2 \text{ and } p = n - 1, \\ T_{n-q} c_{n-q}^2 X_q^* Z_p & \text{for } q \leq n - 1 \text{ and } p = n + 1, \\ T_{q-n} c_{q-n}^1 X_q^* Z_p & \text{for } q \geq n + 1 \text{ and } p = q + 1. \end{cases} \quad (\text{B.6})$$

We note that $L_n(X_p, Y_q, c)$ is related to $Q_n(X, Y, c)$, defined in (3), by

$$Q_n(X, Y, c) = \sum_{p,q} L_n(X_p, Y_q, c). \quad (\text{B.7})$$

Appendix C. Energy transfer results

In figures C.1, C.2 and C.3 the energy transfers are plotted for respectively $P_m = 10^{-3}$, 1 and 10^5 . In each figure the columns from left to right correspond to $\alpha = -\infty, -5/2, -3/2, -1$ and $-1/2$. The rows from the second one to the bottom one correspond to the transfer $\mathcal{T}_{UU}(q, n)$, $\mathcal{T}_{BU}(q, n)$, $\mathcal{T}_{UB}(q, n)$ and $\mathcal{T}_{BB}(q, n)$. The transfers are plotted versus $\log_{10} q$, for three values of n

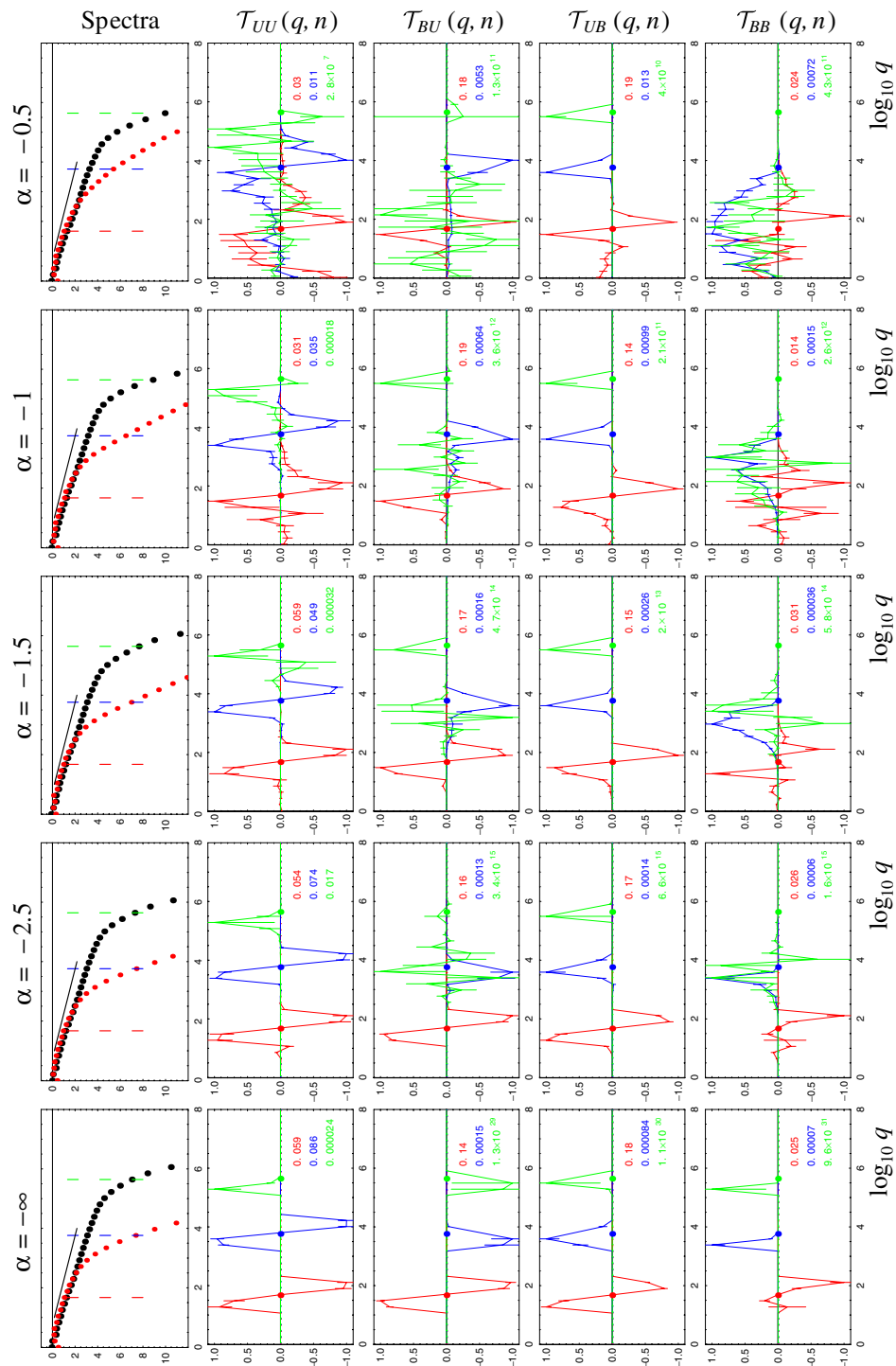


Figure C.1. Spectra and transfer functions for $P_m = 10^{-3}$ ($\nu = 10^{-7}$, $\eta = 10^{-4}$) and several values of α . From left to right column, $\alpha = -\infty$; -2.5 , -1.5 , -1 and -0.5 . From top to bottom, the plots correspond to the spectra (red dots for kinetic and black for magnetic), $\mathcal{T}_{UU}(q, n)$, $\mathcal{T}_{BU}(q, n)$, $\mathcal{T}_{UB}(q, n)$ and $\mathcal{T}_{BB}(q, n)$. For a given α , the transfer functions are plotted versus q for three values of n indicated by the dashed lines.

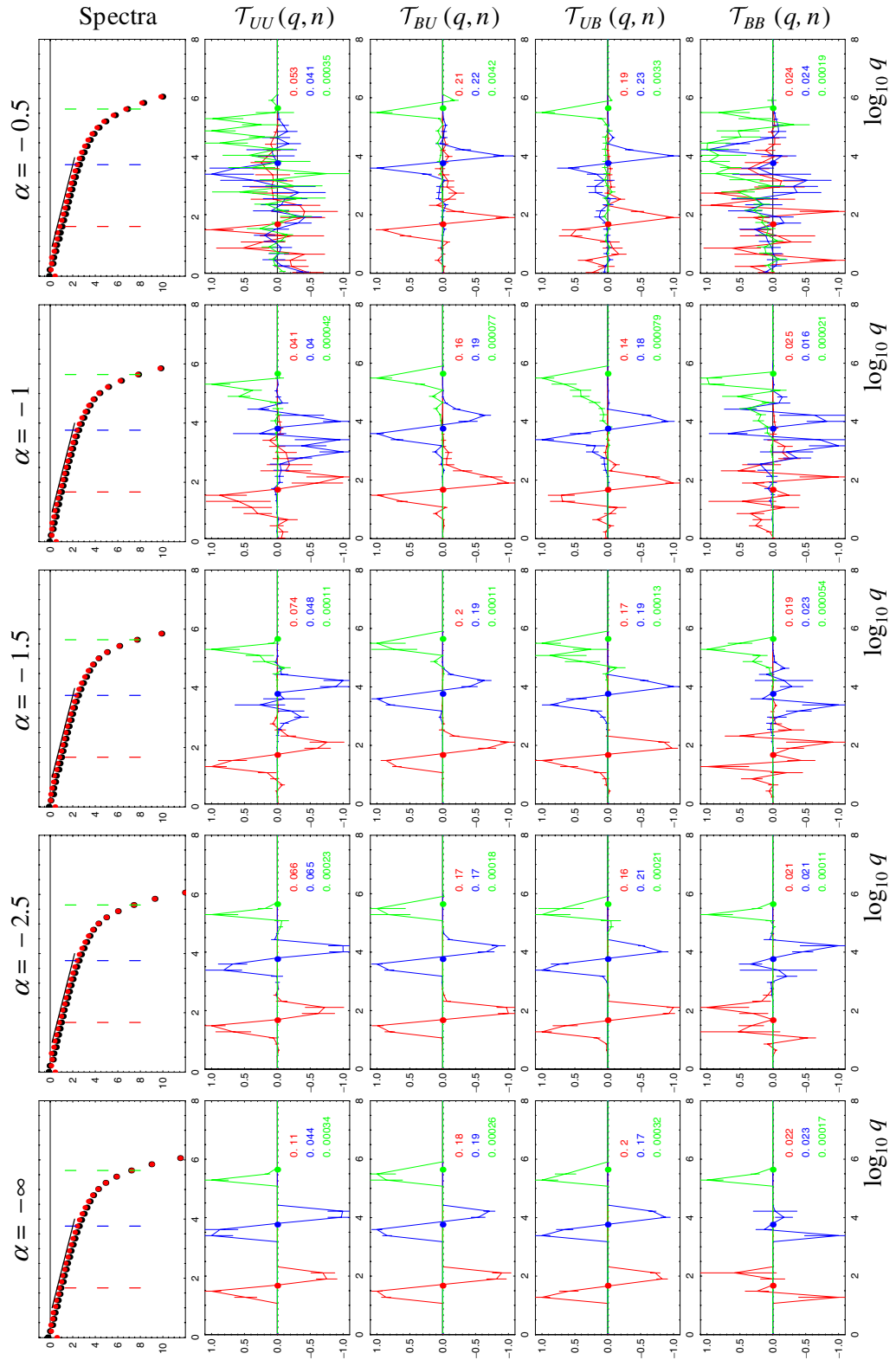


Figure C.2. Same as figure C.1 but for $P_m = 1$ ($\nu = \eta = 10^{-7}$).

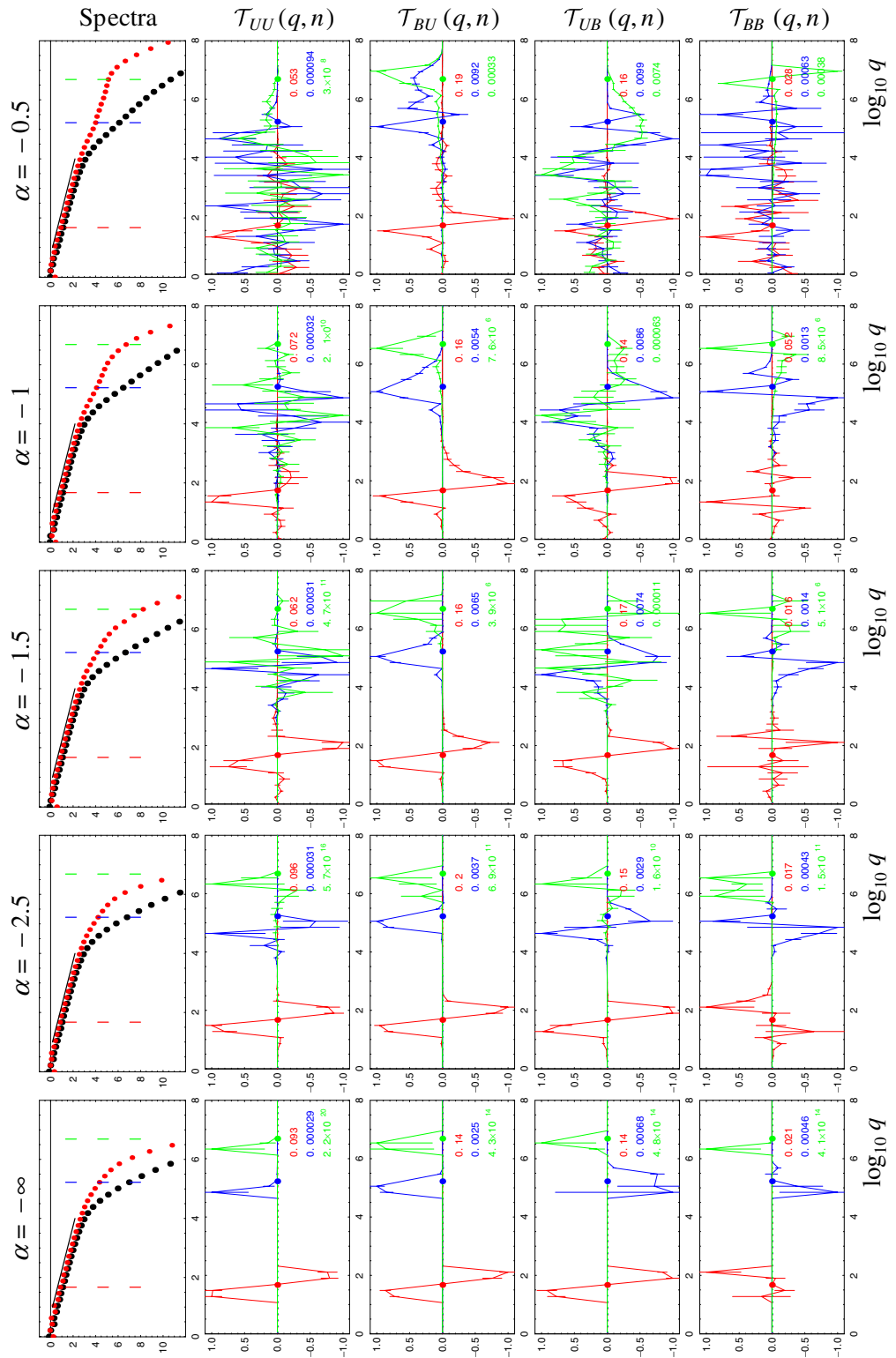


Figure C.3. Same as figure C.1 but for $P_m = 10^5$ ($\nu = 10^{-6}$, $\eta = 10^{-11}$).

which are indicated by the dashed vertical lines on the spectra plots on the top row and by the red, green or blue dots. The transfers being time-dependent we plot their time-average with error bars corresponding to the standard deviation of the mean. This gives some estimation of the robustness of the results. Some quantities are much more noisy than the others and therefore less reliable. The local transfers seem to be always dominant whatever the values of P_m or α . However there is also some evidence of non-local transfers which are discussed in section 3.4.

References

- [1] Obukhov A M 1971 Some general characteristic equations of the dynamics of the atmosphere *Atmos. Oceanic Europhys.* **7** 41
- [2] Lorenz E 1972 Low order models representing realizations of turbulence *J. Fluid Mech.* **55** 545
- [3] Gledzer E B 1973 System of hydrodynamic type admitting two quadratic integrals of motion *Dokl. Akad. Nauk SSSR* **209** 1046
Gledzer E B 1973 *Sov. Phys.—Dokl.* **18** 216 (Engl. Transl.)
- [4] Desnyansky V N and Novikov E A 1974 The evolution of turbulence spectra to the similarity regime *Izv. Akad. Nauk SSSR Fiz. Atmos. Okeana* **10** 127
- [5] Siggia E D 1977 Origin of intermittency in fully developed turbulence *Phys. Rev. A* **15** 1730
- [6] Nakano T 1988 Direct interaction approximation of turbulence in the wave packet representation *Phys. Fluids* **31** 1420
- [7] Yamada M and Ohkitani K 1987 Lyapunov Spectrum of a Chaotic Model of Three-Dimensional Turbulence *J. Phys. Soc. Japan* **56** 4210
- [8] Frisch U 1995 *Turbulence: The Legacy of A N Kolmogorov* (Cambridge: Cambridge University Press)
- [9] Bohr T and Jensen M H and Paladin G and Vulpiani A 1998 *Dynamical Systems Approach to Turbulence* (Cambridge: Cambridge University Press)
- [10] Pope S B 2000 *Turbulent Flows* (Cambridge: Cambridge University Press)
- [11] Biferale L 2003 Shell models of energy cascade in turbulence *Annu. Rev. Fluid Mech.* **35** 441–68
- [12] L’vov V, Podivilov E, Pomlyalov A, Procaccia I and Vandembroucq D 1998 Improved shell model of turbulence *Phys. Rev. E* **58** 1811
- [13] L’vov V, Podivilov E and Procaccia I 1999 Hamiltonian structure of the Sabra shell model of turbulence: exact calculation of an anomalous scaling exponent *Europhys. Lett.* **46** 609
- [14] Ditlevsen P D 2000 Symmetries, invariants and cascades in a shell model of turbulence *Phys. Rev. E* **62** 484
- [15] Benzi R, Biferale L, Tripicciono R and Trovatore E 1996 (1+1)-dimensional turbulence *Phys. Fluids* **9** 2335–63
- [16] Mingshun J and Shida L 1997 Scaling behavior of velocity and temperature in a shell model for thermal convective turbulence *Phys. Rev. E* **56** 441
- [17] Hattori Y, Rubinstein R and Ishizawa A 2004 Shell model for rotating turbulence *Phys. Rev. E* **70** 046311
- [18] Bowman J C, Eckhardt B and Davoudi J 2004 *Spectral Reduction of the Goy Shell Turbulence Model* Online at <http://www.math.ualberta.ca/bowman/talks/caims04.pdf>
- [19] Zimin V and Hussain F 1995 Wavelet based model for small-scale turbulence *Phys. Fluids* **7** 2925
- [20] Melander M 1997 Helicity causes chaos in a shell model of turbulence *Phys. Rev. Lett.* **78** 1456
- [21] Melander M and Fabijonas B 2002 Self similar enstrophy divergence in a shell model of isotropic turbulence *J. Fluid Mech.* **463** 241
- [22] Melander M and Fabijonas B 2003 Transients in the decay of isotropic turbulence *J. Turbul.* **4** 014
- [23] Grappin R, Léorat J and Pouquet A 1986 Computation of the dimension of a model of fully developed turbulence *J. Phys. (France)* **47** 1127
- [24] Gloaguen C, Léorat J, Pouquet A and Grappin R 1985 A scalar model for MHD turbulence *Physica D* **51** 154

- [25] Carbone V 1994 Scale similarity of the velocity structure functions in fully developed magnetohydrodynamic turbulence *Phys. Rev. E* **50** 971
Carbone V 1994 *Europhys. Lett.* **27** 581
- [26] Biskamp V 1994 Cascade models for magnetohydrodynamic turbulence *Phys. Rev. E* **50** 2702
- [27] Frik P 1983 Hierarchical model of two-dimensional turbulence *Magn. Hidrodin.* **19** 60
Frik P 1983 *Magnetohydrodynamics* **19** 48
- [28] Frik P 1984 Two-dimensional MHD turbulence: hierarchical model *Magn. Hidrodin.* **20** 48
Frik P 1983 *Magnetohydrodynamics* **20** 262
- [29] Brandenburg A, Enquist K and Olesen P 1996 Large-scale magnetic fields from hydromagnetic turbulence in the very early universe *Phys. Rev. D* **54** 1291
- [30] Frick P and Sokoloff D 1998 Cascade and dynamo action in a shell model of magnetohydrodynamic turbulence *Phys. Rev. E* **57** 4155
- [31] Stepanov R and Plunian P 2006 Fully developed turbulent dynamo at low magnetic Prandtl number *J. Turbul.* **7** 39
- [32] Hori D, Furukawa M, Ohsaki S and Yoshida P 2005 A shell model for the Hall MHD system *J. Plasma Fusion Res.* **81** 141–2
- [33] Frick P, Stepanov R and Nekrasov V 2002 Shell model of the magnetic field evolution under Hall effect *Magnetohydrodynamics* **39** 327–34
- [34] Kraichnan R H 1965 Inertial-range spectrum of hydromagnetic turbulence *Phys. Fluids* **8** 1385
- [35] Kraichnan R H and Nagarajan R H 1967 Growth of turbulent magnetic fields *Phys. Fluids* **10** 859
- [36] Iroshnikov P S 1963 Turbulence of a Conducting Fluid in a Strong Magnetic Field *Astron. Zh.* **40** 742
Iroshnikov P S 1964 *Sov. Astron.* **7** 566 (Engl. Transl.)
- [37] Verma M K 1999 Mean magnetic field renormalization and Kolmogorov's energy spectrum in magnetohydrodynamic turbulence *Phys. Plasmas* **6** 1455–60
- [38] Haugen N E, Brandenburg A and Dobler W 2003 Is nonhelical hydromagnetic turbulence peaked at small scales? *Astrophys. J.* **597** 141–4
- [39] Schekochihin A A, Cowley S C, Hammett G W, Maron J L and McWilliams J C 2002 A model of nonlinear evolution and saturation of the turbulent mhd dynamo *New J. Phys.* **4** 84
- [40] Schekochihin A A, Maron J L, Cowley S C and McWilliams J C 2002 The small-scale structure of magnetohydrodynamic turbulence with large magnetic Prandtl numbers *Astrophys. J.* **576** 806
- [41] Pouquet A, Frisch U and Léorat J 1976 Strong MHD helical turbulence and the non linear dynamo effect *J. Fluid Mech.* **77** 321–54
- [42] Krause F and Rädler K–H 1980 *Mean-Field Magnetohydrodynamics and Dynamo Theory* (Oxford: Pergamon)
- [43] Alexakis A, Mininni P D and Pouquet A 2005 Imprint of large-scale flows on turbulence *Phys. Rev. Lett.* **95** 264503
- [44] Mininni P D, Alexakis A and Pouquet A 2005 Shell-to-shell energy transfer in magnetohydrodynamics. II. Kinematic dynamo *Phys. Rev. E* **72** 46302
- [45] Carati D, Debliquy O, Knaepen B, Teaca B and Verma M 2006 Energy transfers in forced MHD turbulence *J. Turbul.* **7** 1–12
- [46] Alexakis A, Mininni P D and Pouquet A 2005 Shell-to-shell energy transfer in magnetohydrodynamics. I. Steady state turbulence *Phys. Rev. E* **72** 46301
- [47] Verma M K 2004 Statistical theory of magnetohydrodynamic turbulence: recent results *Phys. Rep.* **401** 229–380
- [48] Brandenburg A and Subramanian K 2005 Astrophysical magnetic fields and non linear dynamo theory *Phys. Rep.* **417** 1–209
- [49] Jensen M H, Paladin G and Vulpiani A 1991 Intermittency in a cascade model for three-dimensional turbulence *Phys. Rev. A* **43** 798
- [50] Pierotti D 1997 Intermittency in the large- n limit of a spherical shell model for turbulence *Europhys. Lett.* **37** 323–8
- [51] Biferale L, Pierotti D and Toschi F 1998 Helicity transfer in turbulent models *Phys. Rev. E* **57** 2515

- [52] Benzi R, Biferale L, Sbragaglia M and Toschi F 2003 Intermittency in turbulence: computing the scaling exponents in shell models *Phys. Rev. E* **68** 046304
- [53] Boffetta G 2002 Lagrangian statistics and temporal intermittency in a shell model of turbulence *Phys. Rev. E* **66** 066307
- [54] Leveque E and She Z-S 1997 Cascade structures and scaling exponents in a dynamical model of turbulence Measurements and comparison *Phys. Rev. E* **55** 2789
- [55] Lesieur M 1997 *Turbulence in Fluids* (Dordrecht: Kluwer)
- [56] Batchelor G K and Townsend A A 1948 Decay of turbulence in the final period *Proc. R. Soc. Lond. A* **194** 527
- [57] Fournier J-D, Sulem P-L and Pouquet A 1982 Infrared properties of forced magnetohydrodynamic turbulence *J. Phys. A: Math. Gen.* **15** 1393